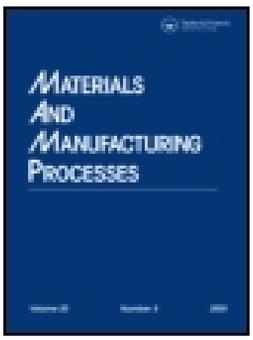

Materials and Manufacturing Processes

ISSN: 1042-6914 (Print) 1532-2475 (Online) Journal homepage: http://www.tandfonline.com/loi/lmmp20

Modeling and Surface Texturing on Surface Roughness in Machining $LaPO_4$-Y_2O_3 Composite

K. Balamurugan, M. Uthayakumar, S. Sankar, U.S. Hareesh & K.G.K. Warrier

To cite this article: K. Balamurugan, M. Uthayakumar, S. Sankar, U.S. Hareesh & K.G.K. Warrier (2017): Modeling and Surface Texturing on Surface Roughness in Machining $LaPO_4$-Y_2O_3 Composite, Materials and Manufacturing Processes, DOI: 10.1080/10426914.2017.1291956

To link to this article: http://dx.doi.org/10.1080/10426914.2017.1291956

Accepted author version posted online: 10 Feb 2017.

Modeling and Surface Texturing on Surface Roughness in Machining $LaPO_4$-Y_2O_3 Composite

K. Balamurugan[1], M. Uthayakumar[1], S. Sankar[2], U.S. Hareesh[2], K.G.K. Warrier[2]

[1]Faculty of Mechanical Engineering, Kalasalingam University, Krishnankoil, India
[2]Material Sciences and Technology Division, National Institute for Interdisciplinary Science and Technology, Council of Scientific and Industrial Research, Thiruvananthapuram, India.

Corresponding Author: M. Uthayakumar E-mail: uthaykumar@gmail.com, m.uthayakumar@klu.ac.in

Received 06 Aug 2016, Revised 05 Jan 2017, Accpeted 09 Jan 2017

Abstract

In this work the Lanthanum phosphate with 20% Yttria ($LaPO_4/Y_2O_3$) composite prepared by Aqueous Sol-Gel process is machined by Abrasive Water Jet Machine (AWJM). The machiniability of this composite is studied by varying the input parameters namely Jet Pressure (JP), Stand-Off Distance (SOD) and Traverse Speed (TS) on Surface finish. Garnet of 80 mesh size is used as abrasive with a flow rate of 85 gms/min. The micro structural characterization study reveals the presence of new element YPO_4. This element enhances the machiniability and reduced porosity in the composite. Microscopy examinations on machined surface reveals that partial overlapping at low JP, poor surface finish at high JP and SOD, Forged deficiency at maximum SOD and TS. The minimum level of all input parameters are influenced to obtain acceptable Ra. Atomic Force Microscopy (AFM) on kerf surface shows micro wear track and peaks. The Multiple Regression Analysis (MRA) is developed for Ra to check the adequacy. From the

Analysis of Variance (ANOVA), SOD has the significant effect on Ra with a contribution of 53%. The influence of JP and TS on Ra is found to be 31% and 15%, respectively.

KEYWORDS: $LaPO_4/Y_2O_3$ composite; Abrasive waterjet machine, Microscopic characterization; Surface topography; Multiple Regression Analysis.

INTRODUCTION

Machining is undeniable in the manufacturing industry. In non-traditional machining technique, AWJM creates its unique advantages over the other machining processes by the ability to machine all materials, ecofriendly, non-heat affected zone on the cut region and almost less load impact on the sample [1]. In AWJM, the high velocity water is pumped from the motor and passed through the mixing chamber. The abrasive gets accelerated and it strikes the specimen with high velocity through the nozzle. AWJM has some disadvantages like noisy operation and a messy operational atmosphere [2]. $LaPO_4$ is identified to have monazite structure and has the ability to withstand even at elevated temperature without any phase transformation [3]. The earlier study of $LaPO_4$ shows that stoichiometric lanthanum phosphate does not react with aluminum and zirconium oxides [4]. The alumina and Zirconia which are found to be tough in machining ceramics get improved its machinability by the addition of $LaPO_4$ [5].

Surface roughness is one of the important parameters which greatly influence product quality and the manufacturing cost of the product [6]. A study on surface roughness of aluminium alloys with varying operating conditions in AWJM has found that material

with high mechanical properties possess low surface roughness value [7]. An adverse effect on surface texture on varying the feed rate is recorded while on machining brass material in AWJ [8]. Intensive jet pressure plays a significant role in the surface texture and material removal rate while machining [9-10]. Surface quality greatly depends on the thickness of the sample in AWJM. Subsurface distortion and strain hardening take place while machining hard materials in AWJM. The study of the traverse speed on the high strength material reveals that the average traverse speed would achieve an optimistic surface finish [11] and material property is one of the factor that greatly affect the Ra [12]. The jet traverse speed has least significance on Ra on hard titanium alloys [13]. Traverse speed and depth of cut are directly relative to each other in affecting the surface performance characteristics [14]. Increase in TS creates the coarse surface plane in the Inconal718 material [15**].** Increase in water pressure significantly affects the surface texture and material removal morphology [16, 17].

Y_2O_3 has high thermal stability and resistance to chemical attack. Hence this compound is used for thermal barrier and corrosion resistance material [18]. An addition of yttria in alumina matrix resists the bulk diffusion and produces a uniform phase [19, 20].The experimental observation in AWJM with different input parameters like JP, SOD and TS on $LaPO_4/Y_2O_3$ composite are investigated. In this paper, the authors are interested to know the surface characteristics of the machined surface of $LaPO_4/Y_2O_3$ composites. The microscopic examination is done on the machined surface and the various mechanisms involve during the machining of this composite are evaluated.

MATERIALS AND METHODS

The calculated amount of lanthanum nitrate is mixed with orthophosphoric acid with the pH of 2 in an ultrasonic bath. The settled precipitate is washed, dried and calcinated to1400^{o}C for 2 hours remove the moisture content in order to get $LaPO_4$. The calcinated powder is mixed with the calculated amount of yttrium nitrite hexahydrate and pH is maintained to 8 by the addition of ammonia. The precipitate settled down is dried and calcinated to remove the wet content and finally the powder is die compacted to get the geometry of 36mm x 7mm at room temperature with a pressure of 480 x 10^6N/m^2. The compacted disc is sintered to 1400^{o}C for 4 hours.

AWJM of Model DIP 6D-2230 is used to cut the $LaPO_4/Y_2O_3$ ceramic composite prepared by Aqueous Sol-Gel process. A 0.25 mm diameter orifice and 0.67 mm diameter WC nozzle is used and the diameter of the nozzle is maintained as same over to the complete observation and after each 10 successive cuts, the nozzle wear is observed. Intensifier unit in AWJM develops the high pressure water of required amount then it is mixed with abrasives in the mixing chamber. The abrasive flow from the hopper is purely on gravity action and the flow rate is found to be 85gms/min. Abrasives gain high acceleration in the mixing chamber. These high velocity abrasive exits through the nozzle and cut the composite. The experimental setup and arrangements of AWJM is shown in Figure 1.

Ra is measured on surf test SJ-411 model of Mitutoyo with the measurement range of 350 μm and with a probe speed of 0.25 mm/sover the length of 5mm. The machined

surface is separated into three sections as top, middle and bottom cut surface. Ra will be the average of these three machined regions and is tabulated. A uniform rectangular cross sectional area of 5 mm x 2 mm for the top, middle and bottom cut surfaces over the machined surface along a vertical line is taken as the measured surface for Ra. The probe is allowed to move perpendicular to the jet direction on the selected area of the machined surface.

Mathematical modeling for predicting the successive data for the given experiment is considered to be the important role in the manufacturing process. All the experiments at the various operating conditions are expected to perform. For modeling purpose, Simple and Multiple Regression Techniques (MRA) are frequently adopted because it relates two or more independent variables and also used for determining the linear and/or nonlinear relationship between dependent and independent variables. Simple regression analysis relates only the most substantial predicted variable among n numbers of independent variables rather than predict the variables. To overcome this MRA, modeling technique is preferred. MRA is a suitable mathematical tool for the research problem which includes one unique metric-dependent variable that is related to more than one metric-independent variable [21]. Here in AWJM, the explanatory variables are JP, SOD and TS and dependent response is Ra. Adequate number of explanatory variables with least of predicted response suits better for MRA. The equation generated by MRA can be generally expressed as in equation 1.

$$Y = \beta_0 + \Sigma_{n=1}^{Z} \beta_i \chi_i + \Sigma_{n=1}^{Z} \beta_{ii} \chi_i^2 + \Sigma_{i<j} \Sigma \beta_{ij} \chi_i \chi_j + \mathcal{E}_i \qquad (1)$$

Where, z = number of factors (3), β_0 = co-efficient (Free Term), β_i = linear effect, β_{ii}= squared effect, β_{ij} = interaction effect and ε = error.

First-order polynomial regressions produce a linear equation with a maximum power of the variable as one. When compared with second-order polynomial, the maximum allowable power of the variable is two and the quadratic equation make the second-order polynomial to be statically significant. With increase in order of the polynomial regression equation will increase the mathematical complexity and also, create least significant effects while in the determination of the relationship between the dependent and the independent variables. The second-order polynomial regression representing the surface roughness (Ra) can be expressed as a function of AWJM parameters such as J_P, S_d and T_s. The general equation 1 can be rewritten as equation 2. This equation generates a correlation between the AWJM input parameters and the output responses. The generated equation is:

$$Y = \beta_0 + \beta_1 J_P + \beta_2 S_d + \beta_3 T_s + \beta_{11} J_P^{\,2} + \beta_{22} S_d^{\,2} + \beta_{33} T_s^{\,2} + \beta_{12} J_P S_d + \beta_{13} J_P T_s + \beta_{23} S_d T_s \quad (2)$$

RESULTS AND DISCUSSION

The mechanical properties of the prepared composite are shown in Table 1. Using densometer and by Archimedes method, the bulk density of the composite is found to be 4.87 g/cm^3 and the theoretical density is found to be 4.95 g/cm^3. The relative density of the composite is calculated as 98.4 %. The material fabricated by powder metallurgy technique has high porous property [22]. The analyazation of diffractogram is performed

using the XRD-X'Pert high score software shows the presence of YPO_4. The elevated sintering temperature of 1400°C ± 10°C makes phosphate and yttria molecules to get a new element of YPO_4. This new element reduces the porosity and makes this composite a suitable thermal barrier material and corrosion resistant material. Hence the addition of yttria in $LaPO_4$ increases the relative density and produces high yield strength. The hardness is measured using micro hardness indentation tester on diamond polished surface of the composite at varying load conditions. The hardness is found to be 5.2 x 10^9 N/m^2 at the maximum load condition of 589 N. The significant increase of yttria particles and the reliant soaking period increase the hardness of the composite.

The flexural strength is computed by equation 3 and it is found in the range of 96±12 MPa composite.

$$\sigma fs = \frac{3FL}{2wh^2} \qquad (3)$$

Where, σfs = flexural strength (N/mm^2), F = Fracture load (N), L = Length between outer supports (mm), w = Specimen width (mm) and h = Specimen height (mm)

In three-point bending test, top surface of the composite has undergone compression failure and bottom surface prove to tensile failure. The microscopic examination on the failure region of the $LaPO_4$-Y_2O_3 composite shows the presence of both transgranular and intergranular failure**.** The fracture portion is shown in Figure 2. The mechanism involved during the failure is grain detachment along the grain and through the grain boundary. This is due to the stress produced by the applied load. The surface shows minor beech mark of the fractured part of the composite surface.

The accelerated abrasive strikes the surface and performs machining. Even in the smooth cutting region, machined surface have high surface roughness. Fewer scratches are created by the abrasives in the cut surface of the composite and most of the scratches observed in the Scanning Electron Microscope (SEM) are in micron level. Optical image on three cutting regions with surface graph is shown in Figure 3(a-c). High accelerated abrasives at superior JP enhance to jet divergence and this influence Ra to great extent. This influence by JP is controlled with low SOD. From Table 3 it is observed that TS has least significant effect in Ra with 15% where its interaction with JP and SOD has significantly low effect. An undesirable effect is produced by JP and SOD on Ra while machining this composite in AWJM. With decrease in distance between the nozzle and the work piece and at high operated water pressure, the accelerated abrasive produces superior Ra [23].

The good matrix reinforcement is formed between the $LaPO_4$ and Y_2O_3. The continuous impingement of abrasive particles at an operating condition of JP at 220 x $10^5 N/m^2$, SOD of 1mm and TS of 20mm/min will lead to the erosion of the composite. The repetitive force creates forged region in the machined surface. Yttria being a hard ceramic element than $LaPO_4$, it withstands the large amount of force and the diverted abrasives wipe away the nearby $LaPO_4$ particles which lead to the forged region. Two such forged regions are shown in Figure 4(a).The presences of yttria particle in the forged region are verified through EDAX and shown in Figure 4(b).

When AWJM is operated at the working condition of JP at 220 x $10^5 N/m^2$, TS at 30mm/min and SOD at 3mm, results in the ploughing of matrix and this is shown in Figure 4(c). A significant contribution on the increase in Ra is observed with increase in operating levels of TS and SOD with constant JP. Increase in SOD may influence to enlarge the width of the water beam due to coanda effect [24]. The breakdown of reinforcement particle due to erosion leads to bulk removal of materials to form crater on the kerf surface. The jet divergence allows the larger kerf taper that possibly increase material removal rate. This effect greatly influences the surface finish with the contribution of 31% which was verified from ANOVA. Figure 4(d) shows the surface finish of the composite at the operating condition of JP at 240 x $10^5 N/m^2$, SOD at 1mm and TS at 20mm/min. It is clear to observe the fine grain with the grain boundary after the jet erosion. Good packing of granule in the machined surface is the evident that the fine bonding is occurred within the matrix.

Machining of composite at the operating condition of JP at 220 x $10^5 N/m^2$, SOD at 3mm and TS at 40mm/min induce micron level wear and partial overlapping regions which is shown in Figure 4(e). At low pressure operating condition, the cyclic impingement of the less accelerated abrasives on the composite surface enhances to create the overlapping region. A typical nozzle arrangement shows the traverse direction of the abrasives on the kerf surface. At maximum level operating condition of TS, surface waviness is formed in the rough cut region and it can be verified by the optical image Figure 3(c). Microscopic image of $LaPO_4/Y_2O_3$ composite machined at the operating of JP of 260 x $10^5 N/m^2$, SOD of 3mm and TS of 40mm/min is shown in Figure 4(f). High level operating condition in

AWJM creates a coarse surface finish. The increase in the thickness of the jet stream irrespective of SOD makes the jet divergence and enhance to material removal rate and kerf angle [25]. Both the transgranular and intergranular failure are observed on the eroded region. The pull out of the reinforcement particles and a typical step type transgranular fracture occurs over the surface is observed in the image. The deep valley (cleavage) created by the abrasive flow on the machined surface prove the machinability of $LaPO_4/Y_2O_3$ composite.

The least observation of Ra from Table 2 is chosen and this cut surface is exposed to AFM and is shown in Figure 5. In Figure 5(a), the high accelerated abrasives give raise to peaks and forged regions. The accelerated abrasive strikes the composite surface and pierces the element. The energy dropped abrasives carried by the back scatter water creates a micro wear marks on the surface. In Figure 5(b) most of the exposed regions appear to be smooth, due to the overlapping effect produced by low JP. The abrasive flow directions are visible and are shown by arrow heads. In Figure 5(c), the peaks obtained are found to be in the range of 75 nm to 90 nm in height due to low SOD and TS, respectively. The spectrum of Ra over the inspected region is shown in Figure 5(d) which exposes the intensity of peak and valley. Most of the inspected region constitute of small peaks and valleys of less than 30 nm.

Initially, three explanatory variables (JP, SOD and TS) with its three varying levels for Ra are tabulated in Table 2. From the observations, it is clear that, for machining the $LaPO_4/Y_2O_3$ composite in AWJM, each independent parameter has produced a

significant effect on Ra. At constant JP and SOD, the influence of TS on Ra is found to be in incremental order. High TS create striations in the rough cut region due to reduced machining time. Similar finding are recorded for JP and SOD. Significant influence on Ra is observed with increase in operating condition of AWJM.

Predicted equation for Ra by MRA is shown as equation 3. The values of R^2 and Adjacent R^2 are identified to be 98.9% and 98.3%, respectively. ANOVA of MRA for Ra shown in Table 3.

$$\begin{aligned} Ra = {} & -10.75 + 0.0582\,JP + 2.453\,SOD - 0.0192\,TS - 0.000039\,JP\ x\ JP \\ & - 0.0238\,SOD\ x\ SOD + 0.000514\,TS\ x\ TS - 0.00638\,JP\ x\ SOD \\ & + 0.000137\,JP\ x\ TS - 0.00063\,SOD\ x\ TS \end{aligned} \quad (3)$$

From the ANOVA, it is identified that the interaction of three explanatory variables of AWJM has no significance on Ra. SOD has a significant effect on Ra with a contribution of 31%, followed by JP of 31% and TS of 15%. The contribution percentage of each individual process parameters on AWJM is shown in Figure 6.

The combined plots between the different sets of independent process variables to Ra are shown in the Figure 7(a-c). From the plots, it is predicted that the increase in all the three process parameters in AWJM tends to increase the Ra. With high level operating condition of JP and SOD expand the thickness of the water beam which leads to produce rough surface finish. At low level operating condition of TS and SOD irrespective of JP enhance the surface finish on the kerf surface. All the experimental values observed are found to be distributed around the predicted value and it is shown in Figure 7(d).

Table 4 shows the response table of Ra by MRA. The three input process parameters predominantly determine the characteristics of Ra with a combined contribution of 97.6%. Owing to a constant value, not much of concentration is done on intercept. At 95% confidential level, less population (total number of experiments) limit tends to take additional attention on T-statistics rather than P-value. T-Inverse value for these explanatory variables at 0.05% significant level with the Degree of freedom (DOF) as 26 is found to be 2.056. The obtained T-Statics observations are found to be lesser than the confidential level. Adjusted square of residual correlates the explanatory variables where the residual square explains only the probability among the explanatory variables. Hence, in the regression statistics observation, the percentage of adjusted square of residual pays attention and is found to be at 98.3% which is at the acceptable level and the residual square is found to be at 98.89%. The addition of input parameters increases the residual square where this tends to decrease the adjusted square of residual. This is observed in regression statistics table during the conformation test. Ra shows a most significant effect under this combination of JP and SOD with contribution of 81.5%. SOD and TS interaction contribute 64.7%. Subsequent increase in thickness of water beam at high JP and SOD, respectively prove to have high significance over SOD and TS. JP and SOD, as individual parameters contributes an effect of 27.7% and 50.5%, respectively over the output response.

To validate the MRA equation, a trial experiment which is not in the experimental design is conducted and presented in Table 5. Three experimental runs are made to validate the repeatability of the presented model. The average of this experimental observation on Ra

is tabulated. The predicted accuracy is found to be 99.12% and it witness the potential applicability and in the trial experiment, an increase of R^2 and Adjusted R^2 by 98.9% and 98.18%, respectively is observed from the regression statistics table.

CONCLUSIONS

The $LaPO_4/Y_2O_3$ ceramic matrix composite by Aqueous Sol-Gel technique was prepared successfully. The following conclusions are drawn from AWJM:

1. Brittle to ductile types of transition fracture is observed showing both transgranular and intergranular on the kerf surface.
2. Erosion of the reinforced yttria particles form crater wear. The repetitive load given by abrasives over the yttria particle tends to deform and break of matrix bond. This enhances the forged deficiency and crater on the kerf surface.
3. JP and SOD are interrelated to each other. One parameter has to set to have low level over the other irrespective of TS. This condition enhances the surface finish on this composite material.
4. Excellent embrittlement and good reinforcement matrix is observed on the kerf surface.
5. From AFM analysis on the kerf surface shows that the peaks formed by the abrasive particles are in the range 75 nm to 90 nm.
6. MRA at 95% confident level over the observed explanatory variables shows that they have significant level of contribution in determination of the surface finish of this new

composite. The obtained MRA equation is verified by the conformation test and it shows the accuracy of 99.12%.

7. Ra is greatly influenced by SOD with 52%. A least significance contributions of JP and TS with 31% and 15%, respectively is observed. However, change in any one independent parameter in AWJM significantly affects Ra value to the greater extent.

8. It is preferred to have a low level operating condition for all input parameters in AWJM for this composite to have an acceptable level of surface finish.

ACKNOWLEDGEMENT

The authors wish to express their thanks to DST-FIST Sponsored Advance Machining and Measurement Laboratory- Kalasalingam University for their support rendered to pursue this research work.

REFERENCES

[1]. Folkes, J. Waterjet-An innovative tool for manufacturing. *Journal of Material Process Technology* **2009**, *209*(20), 6181–6189. doi: 10.1016/j.jmatprotec.2009.05.025.

[2]. Azmir, M.A.; Ahsan, A.K. Investigation on glass/epoxy composite surfaces machined by abrasive waterjet machining. *Journal of Materials Processing Technology* **2008**, *198*(1-3), 122–128. doi: 10.1016/j.jmatprotec.2007.07.014.

[3]. Sankar. S.; Athira. N.R.; Jyothi. C.K.; Warrier. K.G.K.; Padmanabhan. P.V.A. Room temperature synthesis of high temperature stable $LaPO_4$–Yttria nano composite. *Materials Research Bulletin* **2012**, *47*(7), 1835–1837. doi: 10.1016/j.materresbull.2012.03.033.

[4]. Rajesh. K.; Sivakumar. B.; Krishna Pillai. P.; Mukundan. P.; Warrier. K.G.K.; Nair. V.R. Synthesis of nanocrystalline $LaPO_4$ for low temperature densification to monazite ceramics. *Materials Letters* **2004**, *58*(11), 1687–1691. doi: 10.1016/j.matlet.2003.11.028.

[5]. Davis. J.B.; Marshall. D.B.; Morgan. P.E.D. Oxide Composites of Al_2O_3 and $LaPO_4$. *Journal of the European Ceramic Society* **1999**, *19*(13-14), 2421–2426. doi: 10.1016/S0955-2219(99)00112-0.

[6]. Nalbant. M.; Gokkaya. H.; Sur. G. Application of Taguchi method in the optimization of cutting parameters for surface roughness in turning. *Material Design* **2007**, *28*(4), 1379–1385. doi: 10.1016/j.matdes.2006.01.008.

[7]. Tosun. N.; Dagtekin. I.; Ozler. L.; Deniz. A. Abrasive waterjet cutting of aluminum alloys workpiece surface roughness. *Applied Mechanics and Materials* **2013**, *404*, 3–9. doi: 10.4028/www.scientific.net/AMM.404.3.

[8]. Akkurt. A. Cut front geometry characterization in cutting applications of brass with abrasive water jet. *Journal of Materials Engineering and Performance* **2010**, *19*(4), 599–606. doi: 10.1007/s11665-009-9513-8.

[9]. Yuvaraj. N.,Pradeep Kumar. M. Multiresponse Optimization of Abrasive Water Jet Cutting Process Parameters Using TOPSIS Approach. *Materials and Manufacturing Processes* **2014**, *30*(7), 882-890.

[10]. Mittal. S.; Kumar V.; Kumar H. Experimental investigation and optimization of process parameters of Al/Sic MMCs finished by abrasive flow machining. *Materials and Manufacturing Processes* **2015**, *30*(7), 902-911. doi: 10.1080/10426914.2015.1004704.

[11]. Derzija. B.H.; Ahmet. C.; Muhamed. M.; Almina. D. Experimental Study on surface roughness in abrasive water jet cutting. *Procedia Engineering* **2015**, *100*, 394–399. doi: 10.1016/j.proeng.2015.01.383.

[12]. Pirso. J.; Viljus. M.; Juhani. K. Three-body abrasive wear of TiC–Ni Mo cermets. *Tribology International* **2010**, *43*(1-2), 340–346. doi: 10.1016/j.triboint.2009.06.014.

[13]. Fowler. G.; Pashby. I.R.; Shipway P.H. The effect of particle hardness and shape when abrasive water jet milling titanium alloy Ti6Al4V. *Wear* **2009**, *266*(7-8), 613–620. doi: 10.1016/j.wear.2008.06.013.

[14]. Karakurt. I.; Aydin. G.; Aydiner. K. An experimental study on the depth of cut of granite in abrasive waterjet cutting. *Materials and Manufacturing Processes* **2012**, *27*(5), 538–544. doi: 10.1080/10426914.2011.593231.

[15]. Ay. M.; Caydas. U.; Hascalik. A. Effect of traverse speed on abrasive waterjet machining of age Hardened inconel 718 nickel-based superalloy. *Materials and Manufacturing Processes* **2010**, *25*(10), 1160–1165. doi: 10.1080/10426914.2010.502953.

[16]. Uthayakumar. M.; Adamkhan. M.; Thirumalaikumaran. S.; Adam. S.; Jerzy, Z. Machinability of nickel based super alloy by abrasive water jet machining. *Materials and Manufacturing Processes* **2016**, 31(13), 1733-1739. DOI: 10.1080/10426914.2015.1103859.

[17]. Srinivasu. D.S.; Axinte. D.A. Surface integrity analysis of plain waterjet milled advanced engineering composite materials. *Procedia CIRP* **2014**, *13*, 371 – 376. doi: 10.1016/j.procir.2014.04.063.

[18]. Thiyagarajan T.K.; Padmanabhan. P.V.A.; Sreekumar K.P.; Chakravarthy. Y.; Das. A.K.; Gantayet. L.M.; Selvan. B.; Ramachandran. K. Experimental and simulation approach to plasma spray deposition of yttrium oxide. *Surface Engineering* **2012**, *28*(9), 646–656. doi: 10.1179/1743294412Y.0000000019.

[19]. Berger. O.; Boucher. R.; Ruhnow. M. Oxidation of yttrium doped Cr_2AlC films in temperature range between 700 and 1200^{o}C. *Surface Engineering* **2015**, *31*(5), 386–396.

[20]. Ghosh. D.; Mukherjee. S.; Das. S. High temperature oxidation behaviour of yttria (Y_2O_3) coated low alloy steel. *Surface Engineering* **2014**, *30*(7), 524–528. doi: 10.1179/1743294414Y.0000000271.

[21]. Yang. G.; Wang. Z.M.; Cao. Y.; Wang. H.J.; Wei. J.G.; Zhang. J.; Li. X.Y.; Ren. Z.X. Prediction of coal permeability using dimension analysis and multiple regression. *Energy sources, Part A: Recovery, Utilization, and Environmental Effects* **2013**, *35*(16), 1516–1523. doi: 10.1179/1743294414Y.0000000271.

[22]. Ahasan, M.D.; Davidson, M.J. Modelling aspects of hot densification and deformation studies on Al-TiB_2 composite performs. *Materials and Manufacturing Processes* **2015**, *30*(10), 1190–1196. doi: 10.1080/10426914.2015.1019099.

[23]. Selvam. R., Karunamoorthy. L., Arunkumar N. Investigation on performance of abrasive water jet in machining hybrid composites. *Materials and Manufacturing Processes* **2016**, DOI: 10.1080/10426914.2016.1198039.

[24]. Jani. S.P.; Senthil Kumar. A.; Adamkhan. M.; Uthaya Kumar. M. Machinability of hybrid natural fibre composite with and without filler as reinforcement. *Materials and Manufacturing Processes* **2015**, *31*(10), 1393–1399. .doi: 10.1080/10426914.2015.1117633.

[25]. Naresh Babu. M.; Muthukrishnan. N. investigation on surface roughness in abrasive water jet machining by the response surface method. Journal of Materials and Manufacturing Processes 2014, 29 (11-12), 1422–1428. doi: 10.1080/10426914.2014.952020.

Table 1. Properties of $LaPO_4$-Y_2O_3 composite.

S.No	Young's modulus (N/m^2)	Flexural strength (GPa)	Micro Vickers Hardness (GPa)	Theoretical density (g/cm^3)	Experimental density (g/cm^3)	Porosity (%)
1	4.96	96±4	5.2	4.95	4.87	1.1616

Table 2. Experimental observation of Ra and Predicted Ra by MRA at the various working conditions.

S.No	JP ($10^5 N/m^2$)	SOD (mm)	TS (mm/min)	Measured Ra (μm)	Ra by MRA(μm	Error
1	220	1	20	1.664	1.6100	3.2
2	220	1	30	2.074	1.9696	5.0
3	220	1	40	2.482	2.4319	2.0
4	220	2	20	2.613	2.5761	1.4
5	220	2	30	2.826	2.9293	-
6	220	2	40	3.245	3.3853	-4.3
7	220	3	20	3.426	3.4946	-2.0
8	220	3	30	3.816	3.8415	-0.7
9	220	3	40	4.384	4.2912	2.1
10	240	1	20	2.247	2.3425	-4.3
11	240	1	30	2.635	2.7294	-3.6
12	240	1	40	3.098	3.2191	-3.9
13	240	2	20	3.212	3.1811	0.9
14	240	2	30	3.645	3.5617	2.2
15	240	2	40	4.134	4.0450	2.1
16	240	3	20	3.964	3.9721	-0.2
17	240	3	30	4.464	4.3463	2.6
18	240	3	40	4.822	4.8233	-0.0
19	260	1	20	3.141	3.0438	3.0
20	260	1	30	3.459	3.4580	0.0
21	260	1	40	3.980	3.9750	0.1
22	260	2	20	3.601	3.7549	-4.3
23	260	2	30	4.112	4.1628	-1.2
24	260	2	40	4.882	4.6734	4.2
25	260	3	20	4.526	4.4184	2.3
26	260	3	30	4.788	4.8199	-0.7
27	260	3	40	5.142	5.3243	-3.2

Table 3. ANOVA for Ra.

Parameters	DOF	Coefficients	Contribution %	T- Stat	P-value	F-Value
Constant	0	-10.75	98.89%	1.48	0.158	168.01
JP	1	0.05	30.50%	0.98	0.343	0.95
SOD	1	2.45	52.42%	2.15	0.000	26.49
TS	1	-0.01	14.96%	0.37	0.717	0.14
JP X JP	1	-0.00009	0.01%	-0.32	0.756	0.10
SOD X SOD	1	-0.023	0.02%	-0.48	0.637	0.23
TS X TS	1	0.0005	0.07%	1.04	0.313	1.08
JP X SOD	1	-0.006	0.87%	-3.65	0.002	13.29
JP X TS	1	0.0001	0.04%	0.78	0.445	0.61
SOD X TS	1	-0.0006	0.00%	-0.18	0.858	0.03
Error	17		1.11%			
Total	26		100.00%			

Table 4 Response of Actual Ra

Vars	R-Sq	R-Sq (adj)	R-Sq (pred)	JP	SOD	TS
1	52.4	50.5	44.7		X	
1	30.5	27.7	19.1	X		
2	82.9	81.5	78.4	X	X	
2	67.4	64.7	58.6		X	X
3	97.9	97.6	97.0	X	X	X

Table 5. Conformation test result.

S.No	JP ($10^5 N/m^2$)	SOD (mm)	TS (mm/min)	Measured Ra (µm)	Ra by MRA (µm)	Predicted Accuracy (%)
1	260	4	40	6.311	6.255	99.12

Figure 1. Experimental Setup and systematic arrangements of AWJM.

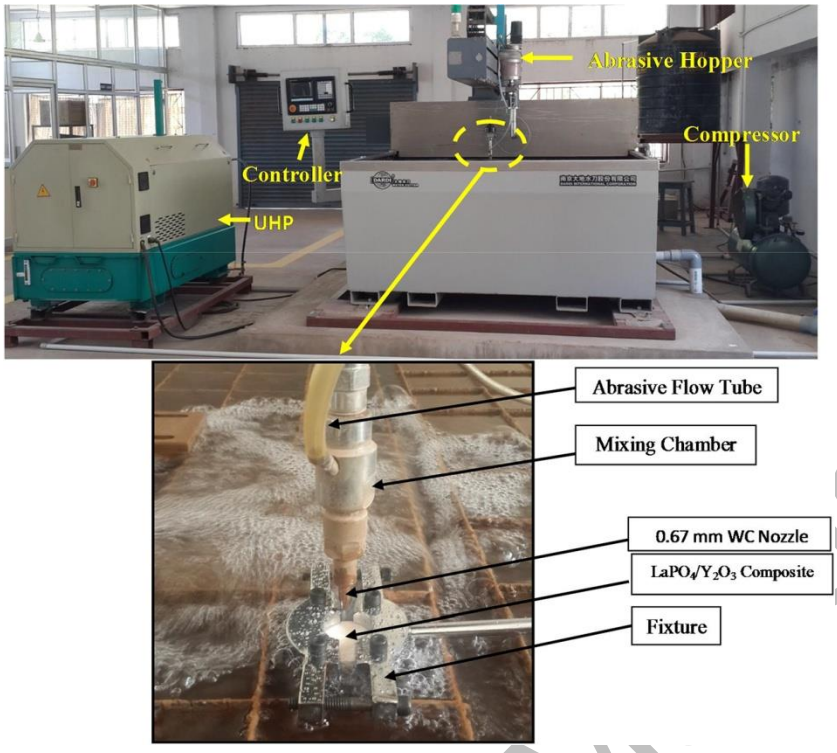

Figure 2. Image on fractured portion of composite.

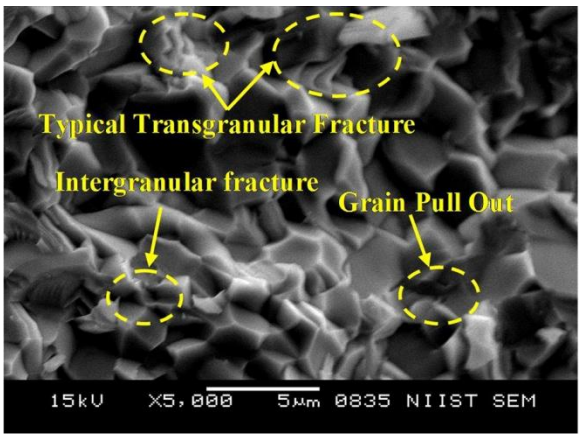

Figure 3. **(a-c)** Optical images on three cutting region with surface graph of Ra.

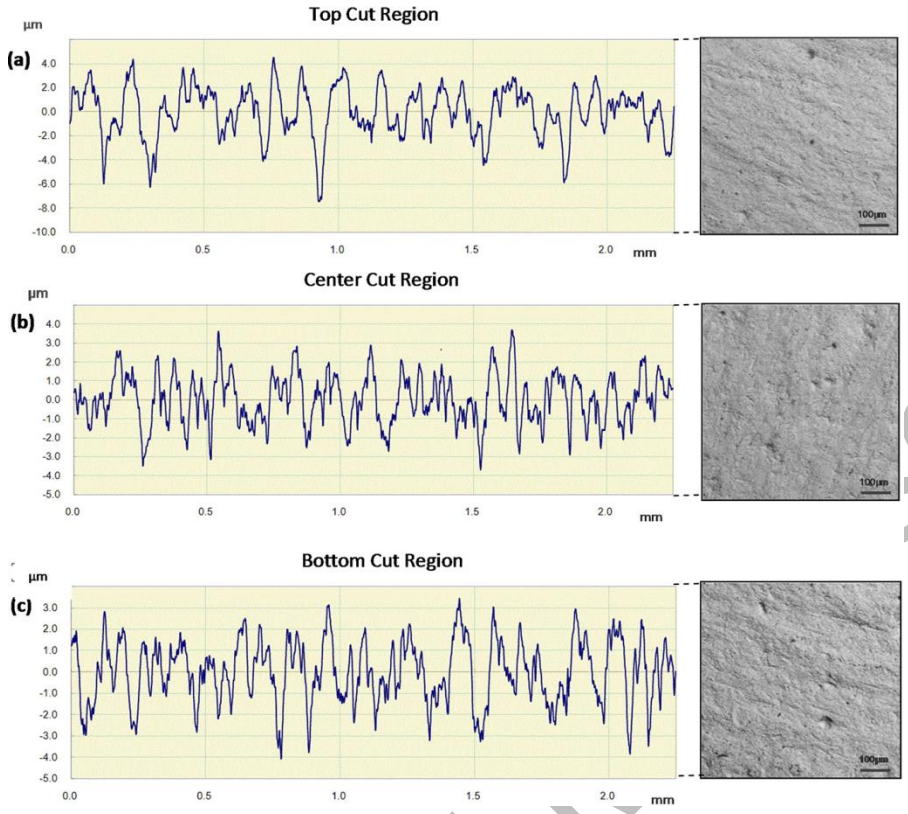

Figure 4. SEM image at various operating conditions in AWJM.

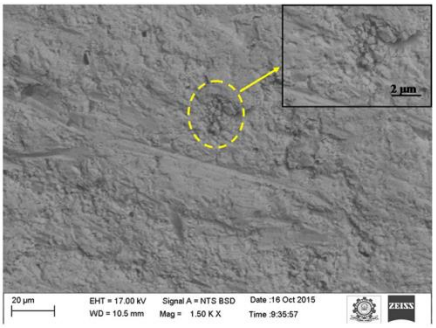

a. Microscopic image at JP=220 x 10^5N/m^2, SOD=1mm and TS=20mm/min and forged region is superimposed.

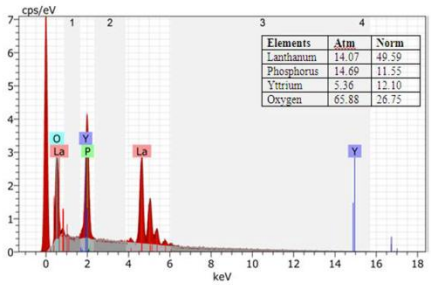

b. EDS spectra of the composite.

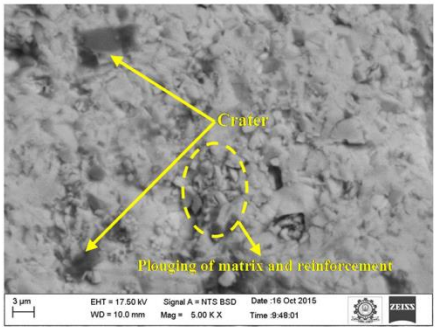

c. Image at JP=220 x 10^5N/m^2, SOD=3mm and TS=30mm/min.

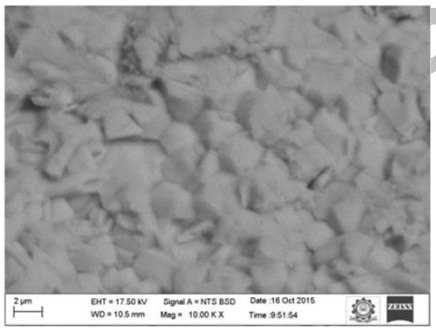

d. Image with fine grain with the grain boundary at operating condition at JP=240 x 10^5 N/m^2, SOD=1mm and TS=20mm/min.

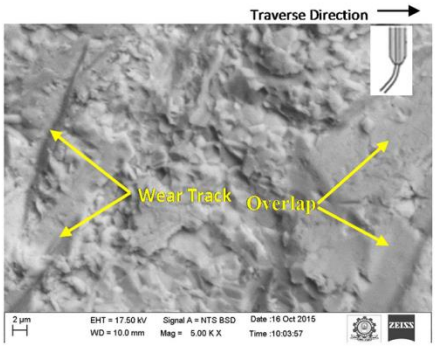

e. Image presenting the direction of flow of abrasives at JP=220 x 105N/m^2, SOD= 3 mm and TS=40mm/min.

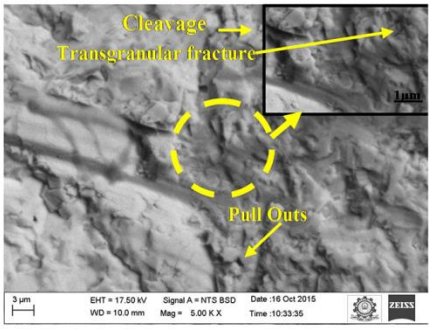

f. Image at JP=260 x 105N/m^2, SOD=3mm and TS=40mm/min and transgranular type failure region is superimposed.

Figure 5. Atomic force microscope images.

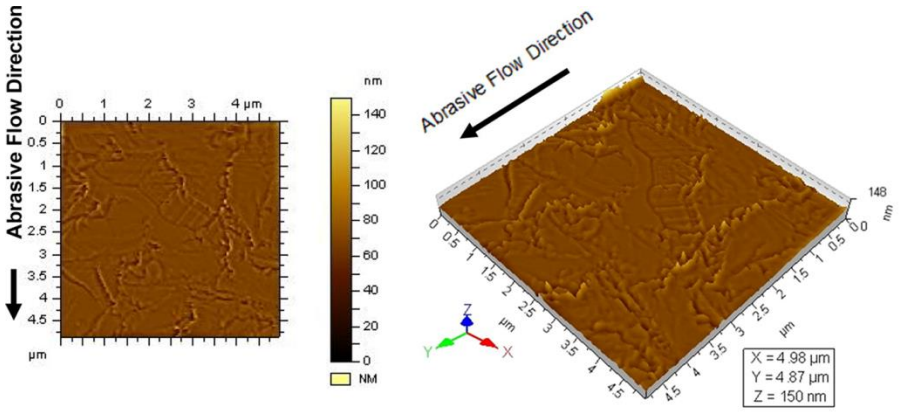

a. 2D image with micro scar.

b. 3D image of the rough cut region.

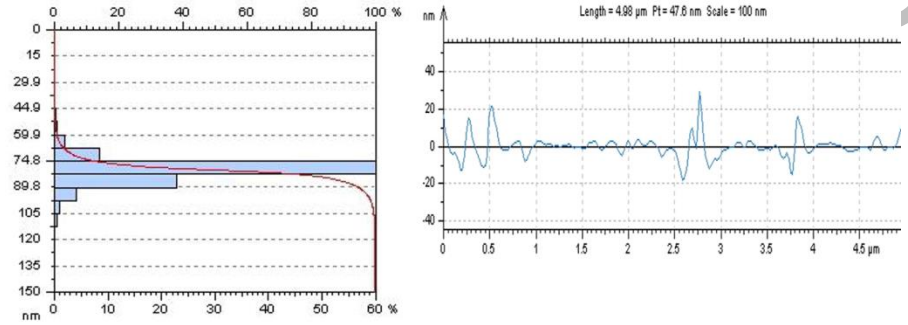

c. Image with peak intensity.

d. Ra graph of the measured face.

Figure 6. The percentage effect of input parameters on Ra

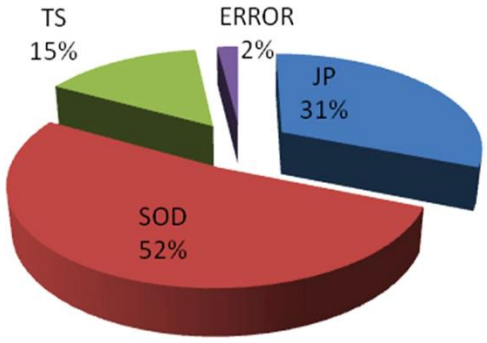

Figure 7. 3-D Plot of three input parameters on Ra

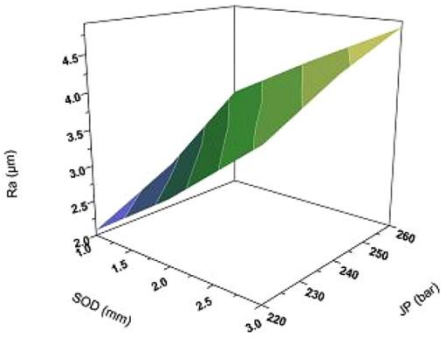

(a) Surface Plot of Actual Ra Vs JP and SOD

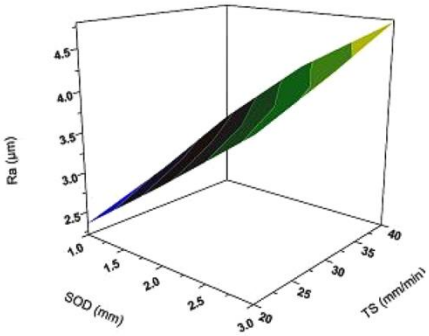

(c) Surface Plot of Actual Ra Vs TS and SOD

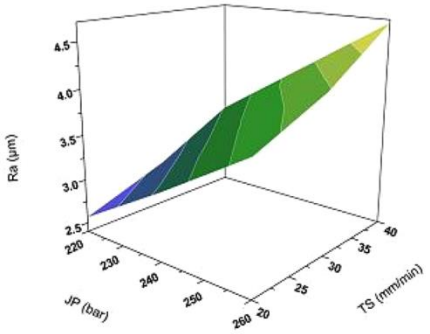

b) Surface Plot of Actual Ra Vs TS and JP

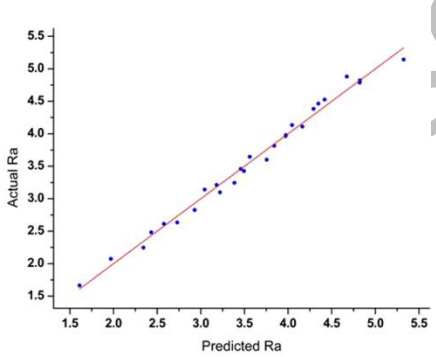

(d) Graph of Predicted Ra Vs Actual